A New Time-Dependent Density-Functional Method for Molecular Plasmonics: Formalism, Implementation, and the $Au_{144}(SH)_{60}$ Case Study

Oscar Baseggio,[a] Martina De Vetta,[a] Giovanna Fronzoni,[a] Mauro Stener,*[a] and Alessandro Fortunelli[b]

We describe the implementation and application of a recently developed time-dependent density-functional theory (TDDFT) algorithm based on the complex dynamical polarizability to calculate the photoabsorption spectrum of large metal clusters, with specific attention to the field of molecular plasmonics. The linear response TDDFT equations are solved in the space of the density fitting functions, so the problem is recast as an inhomogeneous system of linear equations whose resolution needs a numerical effort comparable to that of a SCF procedure. The construction of the matrix representation of the dielectric susceptibility is very efficient and is based on the discretization of the excitation energy, so such matrix is easily obtained at each photon energy value as a linear combination of constant matrix and energy-dependent coefficients. The code is interfaced to the Amsterdam Density Functional (ADF) program and is fully parallelized with standard message passing interface. Finally, an illustrative application of the method to the photoabsorption of the $Au_{144}(SH)_{60}$ cluster is presented.

Introduction

Efficient and accurate prediction of photoabsorption spectra for large systems is a fundamental goal of modern computational research. This goal is usually framed within the time-dependent density-functional theory (TDDFT) formalism, which currently represents a reasonable compromise between accuracy and computational effort. Indeed, TDDFT includes most of the physics present in the photoabsorption phenomenon as concerns electronic motion and is now implemented (in one or other of its variants) in several publicly available quantum chemistry codes. The associated computational cost of this approach can, however, be still very demanding when the size of the system grows larger and larger, and many efforts have been undertaken in research groups to reduce it at a minimum.

In quantum chemistry, an usual procedure is first to solve the Kohn–Sham (KS) equations of density functional theory (DFT) by expanding the molecular KS orbitals as linear combinations of atomic functions, then to recast the TDDFT equations in a form involving the diagonalization of a matrix Ω according to the density matrix formulation of Casida.[1] Therefore, the TDDFT problem is reduced to the extraction of the lowest eigenvalues and eigenvectors of Ω, a matrix whose dimension is the product of the number of occupied and virtual orbitals ($N_{occ} \times N_{virt}$). The dimension of this matrix thus becomes huge for large systems. Such an approach has been implemented in many codes, such as, for example, Amsterdam density functional (ADF),[2–34] and can be made efficient by taking advantages of: (a) the point group molecular symmetry, (b) the Davidson diagonalization iterative algorithm which is well suited for large matrices, (c) electron density fitting techniques through the use of auxiliary basis functions, and finally (d) massive parallelization. This scheme can be computationally feasible on systems containing up to hundreds of atoms, provided one is interested only in the lowest part of the absorption spectrum. However, due to the intrinsic limitation of the Davidson algorithm, which becomes numerically unstable when too many eigenvalues are requested, the higher-energy part of the spectrum of large molecules is basically inaccessible. This situation is encountered for example in the calculation of the photoabsorption spectra of metal clusters which exhibit plasmonic behavior, since the clusters are quite large and the plasmons lie at moderately high energy, so that the number of eigenvalues requested is too high to be practicable using the Davidson algorithm.

To avoid the diagonalization bottleneck, recently a new TDDFT algorithm has been proposed[5] which extracts the spectrum from the calculation of the complex dynamical polarizability. In this approach, the TDDFT equations are projected onto the density fitting auxiliary basis set and therefore the associated numerical problem is recast into the resolution of a nonhomogeneous linear system with a dimension much smaller with respect to the Casida approach. The matrix

[a] O. Baseggio, M. De Vetta, G. Fronzoni, M. Stener
Dipartimento di Scienze Chimiche e Farmaceutiche, Università Di Trieste, via Giorgieri 1, Trieste 34127, Italy
E-mail: stener@univ.trieste.it
[b] A. Fortunelli
CNR-ICCOM, Consiglio Nazionale delle Ricerche, via Giuseppe Moruzzi 1, Pisa 56124, Italia
Contract grant sponsor: MIUR (Programmi di Ricerca di Interesse Nazionale PRIN 2010 DESCARTES).

dimension of such linear system is $k \times (N_{occ} + N_{virt})$ instead of $N_{occ} \times N_{virt}$ of the Casida Ω matrix, with the factor k typically between 1 and 3/2. Moreover, in this new scheme the spectrum at each frequency is obtained as an independent calculation, which makes the algorithm easily parallelizable and feasible essentially for all systems for which a DFT calculation is affordable.

Before describing the new algorithm, which is the topic of the present article, it is worth mentioning other recent alternative TDDFT implementation strategies, which are promising for applications to large systems.

The first one is based on the explicit time-propagation technique. This scheme was introduced in the seminal work of Yabana and Bertsch[6] and is now implemented usually over real space grids, like in the OCTOPUS program,[7] which has been recently applied to study the photoabsorption of large biomolecules[8] and large metal clusters up to 147 atoms[9] and 263 atoms.[10] Real-time TDDFT has been implemented in atomic orbitals codes as well, see Ref. 11 for a recent review.

The second one consists in a superoperator formulation (equivalent to the Sternheimer approach or to the Hylleraas functional) of the TDDFT, which allows the calculation of the dynamical polarizability by means of a very efficient Lanczos method, implemented using plane waves basis set[12]; it has been applied to systems like C_{60}, C_{70}, zinc tetraphenylporphyrin, and chlorophyll-a.[13–15] The Lanczos method is quite appealing for large systems since it furnishes the whole excitation spectrum, at variance with Davidson diagonalization which is limited to the lower part of the spectrum. A third, very recent scheme has been developed by Grimme and consists in a simplified Tamm Dancoff Approximation (TDA)[16] and TDDFT,[17] while a linear-scaling TDDFT has been developed by Zuehlsdorff.[18] A very promising recent method for large systems is the TDDFT time-propagation with transition contribution map (TCM) by Hakkinen[19] which has been employed to calculate the spectrum of clusters containing up to 314 gold atoms protected by ligands. Very recently Nobusada has developed a massively parallel implementation of TDDFT based on real-time and real-space,[20] which allowed to consider clusters containing up to 1414 gold atoms.[21] It is worth noting that each of these algorithms has its different pros and cons. In particular, the Casida algorithm suffers from the already mentioned problem of extracting a large number of eigenvalues, but it has the great advantage of allowing a very detailed assignment of the spectral features in terms of one-electron 1 hole – 1 particle (1h1p) excited configurations. In contrast, the TDDFT algorithms based on time-evolution allow the calculation of the absorption spectrum on a wide energy range; however, they do not give information regarding the nature of the transitions involved in the spectral feature. The only possibility is the inspection of the first-order perturbed density whose nature is useful for a qualitative description but the information gained is too limited to allow a detailed assignment in terms of electronic transitions. Conversely, real-time TDDFT may manifest difficulties in presence of weak interactions between local excited states, in this case very long time are needed to manifest (as in the Förster resonance). At the moment, to the best of our knowledge, for the moment the only method which does not suffer energy limitation and is able to give a detailed assignment is the TDDFT time-propagation with TCM by Hakkinen.[19]

Within already implemented linear response (LR) TDDFT codes, it is worth mentioning also the subsystem formulation of LR-TDDFT[22,23] which is a very promising new idea for future applications on very large systems.

In addition, it should be considered that also the development of highly parallel *ab initio* and DFT codes like NWCHEM[24] is an alternative way to formulate new TDDFT algorithms able to describe large systems. This way appears a practical and promising one, thanks to the increased availability of massively parallel supercomputers.

The article is organized as follows. In method and implementation sections, the Method and its Implementation are described in detail. The Computational Details are reported in computational details section, Application: the $Au_{144}(SH)_{60}$ cluster section is devoted to the application of the present method to study the photoabsorption of the $Au_{144}(SH)_{60}$ cluster, finally, the conclusions are summarized in Conclusions section.

Method

The present formulation is based on calculation of the photoabsorption spectrum $\sigma(\omega)$ point by point from the imaginary part of the dynamical polarizability $\alpha(\omega)$

$$\sigma(\omega) = \frac{4\pi\omega}{c} \Im[\alpha(\omega)] \tag{1}$$

This expression is of practical interest when the polarizability is calculated for complex frequency, that is, $\omega = \omega_r + i\omega_i$, where the real part ω_r is the scanned photon frequency (energy) and ω_i is the imaginary part which corresponds to a broadening of the discrete lines and can be interpreted as a pragmatic inclusion of the excited states finite lifetime.

Now, it will be shown that it is possible to calculate efficiently the complex $\alpha(\omega)$ introducing some approximations. First let us start with the definition:

$$\alpha_{zz}(\omega) = \int \rho_z^{(1)}(\omega, \bar{r}) z d\bar{r} \tag{2}$$

Where $\alpha_{zz}(\omega)$ is the zth diagonal term of the polarizability tensor, $\rho_z^{(1)}(\omega, \bar{r})$ stands for the Fourier component of a given frequency of the first-order time-dependent induced density by the external time-dependent electromagnetic field. For the calculation of the spectrum, the isotropic part of the tensor is actually extracted from the trace: $\alpha(\omega) = \frac{1}{3}\sum_{i=1}^{3} \alpha_{ii}(\omega)$ where the index i runs on the three components x, y, and z.

For the TDDFT, the induced density can be calculated from the KS dielectric susceptibility $\chi_{KS}(\omega, \bar{r}, \bar{r}')$ of a reference system of noninteracting electrons under the effect of an effective perturbing potential $V_{SCF}^{z}(\omega, \bar{r})$ sum of the external potential plus the Coulomb and XC response potential.

This is summarized by the following coupled linear equations:

$$\rho_z^{(1)}(\omega,\bar{r}) = \int \chi_{KS}(\omega,\bar{r},\bar{r}')V_{SCF}^z(\omega,\bar{r}')d\bar{r}' \quad (3)$$

$$V_{SCF}^z(\omega,\bar{r}) = V_{EXT}^z(\omega,\bar{r}) + \int \frac{\rho_z^{(1)}(\omega,\bar{r}')d\bar{r}'}{|\bar{r}-\bar{r}'|} + \frac{\partial V_{XC}}{\partial\rho}\Big|_{\rho^0}\rho_z^{(1)}(\omega,\bar{r}) \quad (4)$$

In last expression, the adiabatic local density approximation (ALDA)[25] has been employed (XC kernel local in time and additionally also in space, V_{XC} is the same for the Casida formulation) and $V_{EXT}^z(\omega,\bar{r})$ corresponds in practice to the z dipole component.

Now, rewrite expressions for the induced density and the perturbing potential in operatorial form:

$$\rho_z^{(1)} = \chi_{KS}V_{SCF}^z \quad (5)$$

$$V_{SCF}^z = V_{EXT}^z + K\rho_z^{(1)} \quad (6)$$

Where in expression (6) K stands for the sum of the Coulomb and the XC kernels:

$$K(\bar{r},\bar{r}') = K_C(\bar{r},\bar{r}') + K_{XC}(\bar{r},\bar{r}') = \frac{1}{|r-r'|} + \delta(r-r')\frac{\partial V_{XC}}{\partial\rho}\Big|_{\rho^0} \quad (7)$$

Due to the linearity of (5) and (6) it is possible to eliminate V_{SCF}^z and to obtain an equation for $\rho_z^{(1)}$ which reads:

$$[1-\chi_{KS}K]\rho_z^{(1)} = \chi_{KS}V_{EXT}^z \quad (8)$$

Now, it is convenient to represent Eq. (8) over a basis set and since the unknown term corresponds to the induced density, it is natural to choose the auxiliary density fitting functions f_μ as basis set. More precisely it is even better to choose such basis as a subset of the fitting set, since the induced density will be affected mainly by valence orbitals so all the functions needed to fit the core density should be excluded without losing of accuracy. With this representation $\rho_z^{(1)}(\omega,\bar{r}) = \sum_\mu^K f_\mu(\bar{r})b_\mu(\omega)$, the following non-homogeneous system of linear algebraic equations is obtained, which written in matrix formulation reads:

$$[\boldsymbol{S}-\boldsymbol{M}(\omega)]\boldsymbol{b} = \boldsymbol{d} \quad (9)$$

Where **S** is the overlap matrix between fitting functions, **b** is the unknown vector with the expansion coefficients $b_\mu(\omega)$ of $\rho_z^{(1)}$, **d** is the frequency-dependent vector corresponding to the known nonhomogeneous term, whose components are:

$$d_\mu = \langle f_\mu|\chi_{KS}(\omega)|z\rangle \quad (10)$$

and finally, the elements of the frequency-dependent matrix **M** are:

$$M_{\mu\nu} = \langle f_\mu|\chi_{KS}(\omega)K|f_\nu\rangle \quad (11)$$

Now, let us analyse the efforts needed to build the frequency-dependent $\boldsymbol{M}(\omega)$ matrix: apparently this is a prohibitive task for a practical calculation, since it should be repeated for each frequency. The original characteristic of the present new method is the introduction of a simple approximation which should enable the construction of $\boldsymbol{M}(\omega)$ as a linear combination of frequency-independent matrices $\boldsymbol{G}^k$ with frequency-dependent coefficients $s_k(\omega)$, with this expression:

$$\boldsymbol{M}(\omega) = \sum_k s_k(\omega)\boldsymbol{G}^k \quad (12)$$

with this idea a set of matrices $\{\boldsymbol{G}^k\}$ is calculated and stored once at the beginning, then the matrix $\boldsymbol{M}(\omega)$ is calculated very rapidly at each photon energy ω.

Now, let us justify the expression (12), starting with the expression of the KS dielectric susceptibility:

$$\begin{aligned}\chi_{KS}(\omega,\bar{r},\bar{r}') &= \sum_i^{Nocc}\sum_a^{Nvirt}\varphi_i(\bar{r})\varphi_a(\bar{r})\frac{4\varepsilon_{ia}}{\omega^2-\varepsilon_{ia}^2}\varphi_i(\bar{r}')\varphi_a(\bar{r}') \\ &= \sum_i^{Nocc}\sum_a^{Nvirt}\Theta_{ia}(\bar{r})\lambda_{ia}(\omega)\Theta_{ia}(\bar{r}')\end{aligned} \quad (13)$$

where in (13) we have assumed real KS occupied φ_i and virtual φ_a orbitals and $\varepsilon_{ia} = \varepsilon_a - \varepsilon_i$ are differences between virtual and occupied KS eigenvalues. Now, consider carefully the right-hand side of expression (13): the frequency dependence enters only in the $\lambda_{ia}(\omega)$ factor, which is "almost" constant for all the pairs of index *i*- and *a*- for which $\varepsilon_a - \varepsilon_i$ is almost constant. This happens when many ε_{ia} are close together, that is when the density of "zero order" excitation energies is high. This important observation allows to profitably change the double sum in expression (13).

In fact, let us consider the distribution of all the ε_{ia} on the excitation energy axis, like in the next Figure 1, and define an energy grid over this axis, starting from the minimum ε_{ia} which corresponds to $\varepsilon_{LUMO} - \varepsilon_{HOMO}$. The energy grid consists of $P+1$ knots $\{E_k\}_{k=1,\ldots,P+1}$ and P intervals I_k.

Now, it is possible to change the double sum of previous Eq. (13) as follows:

$$\chi_{KS}(\omega,\bar{r},\bar{r}') = \sum_{k=1}^{P}\sum_{\varepsilon_{ia}\in I_k}\Theta_{ia}(\bar{r})\lambda_{ia}(\omega)\Theta_{ia}(\bar{r}') \quad (14)$$

the advantage of this new double sum is that, if the energy knots are dense enough, the values of ε_{ia} within each interval can be considered, with good approximation, almost constant and equal to the average $\bar{E}_I = \frac{E_I+E_{I+1}}{2}$: this allows to bring the $\lambda_{ia}(\omega)$ factor outside the inner sum:

$$\chi_{KS}(\omega,\bar{r},\bar{r}') = \sum_{k=1}^{P}\frac{4\bar{E}_k}{\omega^2-\bar{E}_k^2}\sum_{\varepsilon_{ia}\in I_k}\Theta_{ia}(\bar{r})\Theta_{ia}(\bar{r}') \quad (15)$$

so in expression (15) the frequency-dependent dielectric susceptibility is a linear combination of frequency-independent objects (the inner sum) while only the coefficients are frequency dependent. Moreover, if one is interested in the lowest part of the spectrum as usually it happens, the sum in (15) can be safely truncated at a maximum energy cut-off, which can be chosen checking the convergence of the results with respect to such energy cut-off.

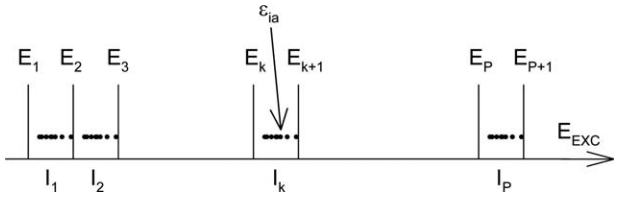

Figure 1. Distribution of the eigenvalue differences over the energy grid for the efficient calculation of the dielectric susceptibility. See text for details. Reprinted from Ref. [5] with the permission of AIP Publishing.

This resummation is the central idea of the present algorithm. Now, we will use this approach to build the matrix $\boldsymbol{M}(\omega)$. From Eq. (11) and using expression (15) we get:

$$M_{\mu\nu}=\sum_{k=1}^{P} s_k(\omega)\sum_{\varepsilon_{ia}\in I_k}\langle f_\mu|\Theta_{ia}(\bar{r})\rangle\langle\Theta_{ia}(\bar{r}')|K|f_\nu\rangle=\sum_{k=1}^{P} s_k(\omega)G^k_{\mu\nu} \quad (16)$$

which now justifies previous expression (12), defines the matrix $G^k_{\mu\nu}$ and the coefficients:

$$s_k(\omega)=\frac{4\bar{E}_k}{\omega^2-\bar{E}_k^2} \quad (17)$$

The construction of each $G^k_{\mu\nu}$ matrix corresponds to a matrix–matrix product:

$$G^k_{\mu\nu}=\sum_{\varepsilon_{ia}\in I_k}\langle f_\mu|\Theta_{ia}(\bar{r})\rangle\langle\Theta_{ia}(\bar{r}')|K|f_\nu\rangle=\sum_{\varepsilon_{ia}\in I_k}A^k_{\mu,ia}B^k_{ia,\nu} \quad (18)$$

Where the matrices **A** and **B** are:

$$A^k_{\mu,ia}=\langle f_\mu|\Theta_{ia}(\bar{r})\rangle \quad (19)$$

$$B^k_{ia,\nu}=\langle\Theta_{ia}(\bar{r}')|K|f_\nu\rangle=\langle\Theta_{ia}(\bar{r}')|\frac{1}{|\bar{r}'-\bar{r}''|}|f_\nu\rangle+\langle\Theta_{ia}(\bar{r}')|\frac{\partial V_{XC}}{\partial\rho}|f_\nu\rangle \quad (20)$$

Finally, from the coefficients b_μ, solution of the Eq. (9), it is possible calculate the dynamic polarizability:

$$\alpha_{zz}(\omega)=\sum_\mu b_\mu\int f_\mu z d\bar{r} \quad (21)$$

Having obtained the components of the complex dynamic polarizability, from expressions (2) and (1) the spectrum is calculated.

Implementation

The new TDDFT algorithm is based on the resolution of the system of linear algebraic Eq. (9), now the construction for the all terms of Eq. (9) will be outlined.

This algorithm has been developed starting from the ADF code,[2,3] in fact many integrals are already calculated by ADF, so the ADF code has been only modified to save these integrals on external files which will be read by an independent program which will complete the calculations.

The ADF code calculates and saves the following analytic integrals:

- The density fitting overlap matrix *S*:

$$S_{\mu\nu}=\langle f_\mu|f_\nu\rangle \quad (22)$$

- Density fitting Coulomb integrals matrix *F*:

$$F_{\mu\nu}=\langle f_\mu|\frac{1}{|\bar{r}'-\bar{r}''|}|f_\nu\rangle \quad (23)$$

- The integrals between two basis functions and one fitting functions (pair fitting) with at least one common center:

$$\langle f_\mu|\sigma\tau\rangle \quad (24)$$

- Dipole integrals between basis functions:

$$\langle\sigma|z|\tau\rangle \quad (25)$$

ADF also saves the molecular orbitals eigenvalues and expansion coefficients.

Finally, we had to implement in ADF also the calculation of new integrals, between fitting functions and the ALDA exchange correlation Kernel:

$$Z_{\mu\nu}=\langle f_\mu|\frac{\partial V_{XC}}{\partial\rho}|f_\nu\rangle \quad (26)$$

The new program reads the files, selects the fitting functions, builds all the needed matrices and solves the TDDFT Eq. (9), calculates the spectrum and performs the analysis.

The new program first builds the energy grid, distributes the difference of eigenvalues between occupied and virtual molecular orbitals, and selects the fitting functions. Then, it builds the matrix A^k:

$$A^k_{\mu,ia}=\langle f_\mu|\varphi_i\varphi_a\rangle=\sum_{\sigma\tau}^{\text{basis}}\langle f_\mu|\sigma\tau\rangle c_{\sigma i}c_{\tau a} \quad (27)$$

The complete calculation of (27) would be far prohibitive, but in ADF a very efficient "pair fitting" technique has been already developed so the run of the basis indexes is not free but limited such that at least one basis function lies on the same center of the fit function. This step will be the most expensive in the matrix construction. The similar procedure is used to calculate the matrix B^k.

$$B^k_{ia,\nu}=\langle\varphi_i\varphi_a|\frac{1}{|\bar{r}'-\bar{r}''|}|f_\nu\rangle+\langle\varphi_i\varphi_a|\frac{\partial V_{XC}}{\partial\rho}|f_\nu\rangle \quad (28)$$

Now, consider the first term of Eq. (28), and exploiting the resolution of the identity:

$$\langle\varphi_i\varphi_a|\frac{1}{|\bar{r}'-\bar{r}''|}|f_v\rangle=\sum_{\gamma\eta}\langle\varphi_i\varphi_a|f_\gamma\rangle S^{-1}_{\gamma\eta}\langle f_\eta|\frac{1}{|\bar{r}'-\bar{r}''|}|f_v\rangle=\left(\left(A^k\right)^+S^{-1}F\right)_{ia,v} \tag{29}$$

The second term of (28) can be calculated in a similar fashion:

$$\langle\varphi_i\varphi_a|\frac{\partial V_{XC}}{\partial\rho}|f_v\rangle=\sum_{\gamma\eta}\langle\varphi_i\varphi_a|f_\gamma\rangle S^{-1}_{\gamma\eta}\langle f_\eta|\frac{\partial V_{XC}}{\partial\rho}|f_v\rangle=\left(\left(A^k\right)^+S^{-1}Z\right)_{ia,v} \tag{30}$$

Therefore, from (28)–(30) we get:

$$B^k_{ia,v}=\left(\left(A^k\right)^+S^{-1}(F+Z)\right)_{ia,v} \tag{31}$$

From previous expression (18) the matrix G^k is defined as follows:

$$G^k=A^kB^k \tag{32}$$

Actually B^k is not directly calculated, but rather matrices D^k and L, whose definitions are:

$$D^k=A^k\left(A^k\right)^+ \tag{33}$$

$$L=S^{-1}(F+Z) \tag{34}$$

We should observe that matrix L is independent from k index (interval energy), so G^k is more conveniently defined in this way:

$$G^k=D^kL \tag{35}$$

Also in this case the matrix G^k is not directly calculated, because it is not computationally convenient, because matrix $M(\omega)$ is obtained as follows:

$$M(\omega)=\sum_{k=1}^{P}s_k(\omega)G^k=\sum_{k=1}^{P}s_k(\omega)D^kL=\left(\sum_{k=1}^{P}s_k(\omega)D^k\right)L \tag{36}$$

Where the coefficients s_k correspond to:

$$s_k(\omega)=\frac{4\bar{E}_k}{\omega^2-\bar{E}_k^2} \tag{37}$$

We have still to calculate the d vector of Eq. (9), that is, the nonhomogeneous term, taking advantages of the previously described technique, it is straightforward:

$$d_\mu=\langle f_\mu|\chi_{KS}(\omega)|z\rangle=\sum_{k=1}^{P}s_k(\omega)\sum_{\varepsilon_{ia}\in I_k}A^k_{\mu,ia}\langle\varphi_i|z|\varphi_a\rangle \tag{38}$$

The dipole moment integrals are calculated with linear combination from integrals (25):

$$\langle\varphi_i|z|\varphi_a\rangle=\sum_{\sigma\tau}^{\text{basis}}\langle\sigma|z|\tau\rangle c_{\sigma i}c_{\tau a} \tag{39}$$

So vector d is easily calculated at each frequency as a linear combination of frequency-independent vectors, accessible from A matrix and conventional dipole matrix elements.

Finally, the complex dynamic polarizability components are calculated:

$$\alpha_{zz}(\omega)=\int\rho_z^{(1)}(\omega,\bar{r})z d\bar{r}=\sum_\mu b_\mu\int f_\mu z d\bar{r}=\sum_\mu b_\mu n_\mu \tag{40}$$

Where the vector b in (40) is the solution of Eq. (9) and the elements of the vector n are integrals which are easily calculated analytically.

This step concludes the calculation of the dynamic polarizability, and therefore of the spectrum, and furnished the first-order TD density which can be used to analyze and rationalize the results. However, our goal is to get also a more complete analysis of the spectrum, namely in terms of linear combination of one-electron excited configurations or in terms of TCMs.[19] To obtain this, it is convenient adopt the modified Sternheimer approach formulation[26] of LR, which furnishes the first-order perturbation of the KS orbitals:

$$\begin{aligned}\left[H^0_{KS}-\varepsilon_i-\omega\right]\varphi_i^{(1,-)}&=-V_{SCF}\varphi_i\\ \left[H^0_{KS}-\varepsilon_i+\omega\right]\varphi_i^{(1,+)^*}&=-V_{SCF}\varphi_i\end{aligned} \tag{41}$$

from the perturbed orbitals the perturbed density is obtained:

$$\rho^{(1)}=2\sum_i^{\text{occ}}\varphi_i\left(\varphi_i^{(1,-)}+\varphi_i^{(1,+)}*\right) \tag{42}$$

It is worth noting that, for convenience, the second inhomogeneous Eq. (41) is actually the complex conjugate with respect to that reported in Ref. [26] for $\varphi_i^{(1,+)}$. Eqs. (41) and (42) in the past were used to calculate self-consistently the V_{SCF} (see the theory chapter) in old TDDFT implementations,[27,28] but in the present context they are useful to easily get the analysis in terms of one-electron configurations once the TDDFT equations have been already solved. In fact if the perturbed orbitals are expanded in terms of virtual KS orbitals the term in brackets is diagonal:

$$\begin{aligned}[\varepsilon_a-\varepsilon_i-\omega]c_i^{a-}&=-\langle\varphi_a|V_{SCF}|\varphi_i\rangle\\ [\varepsilon_a-\varepsilon_i+\omega]c_i^{a+*}&=-\langle\varphi_a|V_{SCF}|\varphi_i\rangle\end{aligned} \tag{43}$$

The polarizability is then expressed by:

$$\alpha_{zz}(\omega)=2\sum_i^{\text{occ}}\sum_a^{\text{virt}}\langle\varphi_i|z|\varphi_a\rangle\left(c_i^{a+*}+c_i^{a-}\right)=\sum_i^{\text{occ}}\sum_a^{\text{virt}}\langle\varphi_i|z|\varphi_a\rangle P_i^a \tag{44}$$

where in Eq. (44), the density matrix (dipole amplitudes) P_i^a is introduced. From Eq. (43) and using the definition of $s_k(\omega)$, we obtain:

$$P_i^a=s_k(\omega)\langle\varphi_i|V_{SCF}|\varphi_a\rangle \tag{45}$$

In practice from imaginary part of Eq. (44) the absorption spectrum is obtained and therefore from imaginary part of expression (45) the analysis in terms of one-electron excited configurations and TCM is obtained.

The dipole amplitudes are actually calculated as follows:

$$P_i^a = s_k(\omega)\left[\langle\varphi_i|z|\varphi_a\rangle + \sum_{\mu\tau}^{fit}\left(A^k\right)^{+}_{ia,\mu} L_{\mu\tau} b_\tau\right] \quad (46)$$

We have decided to implement the new code in a separate program independent by ADF to exploit more easily the parallelization, with the goal to obtain a code that is massively parallel and easily portable on different architectures. For this reasons, we have used standard message passing interface, Basic Linear Algebra Communication Subprograms (BLACS), and ScaLAPACK libraries. The general scheme of the parallel calculation consists of four points: first is the initialization the BLACS grid; second, the distribution of the matrix among the grid processes (typically cyclic block distribution); third, the call to ScaLAPACK routines (matrix product, matrices sum, etc.), fourth the harvest of the results. However, the inclusion of the complete program within the ADF suite is under consideration and will be available in a future release of ADF.

The new program allows a simple choice of a subset of the ADF fitting functions, to save computer time when some fitting functions are not necessary for an accurate description of the photoabsorption spectrum. The strategy to choose a properly reduced fitting subset consists to perform some preliminary TDDFT test calculations on simple systems (typically biatomic molecules) increasing gradually the number of fit functions. Typically this procedure converges rather rapidly, giving calculated spectra that match better and better with those obtained with a standard TDDFT calculation by ADF. When a good match is obtained, the fitting subset of the corresponding atoms can be used for more complicated or larger system.

Of course, the problem of properly choosing the density fitting is not trivial at all, and in the present case it is hampered by the Slater nature of the basis. In this respect, the choice of Gaussian basis set would be more convenient, since it allows a straightforward calculations of the three-center integrals needed to fit the density and can benefit of very efficient implementations.[29]

Equation (9) must be solved for each nonequivalent dipole component, and the induced density $\rho^{(1)}$ must integrate to zero over space due to orthogonality of occupied-virtual orbitals. This condition is naturally satisfied when the dipole component is not totally symmetric, conversely when the symmetry is low and one or more dipole components are totally symmetric, such constrain must be imposed. This is easily done by Lagrange multipliers technique after Eq. (9) is solved. This can be formally realized introducing the constrain and the multiplier λ in (9):

$$\begin{pmatrix} S-M & \cdots & \bar{n} \\ \vdots & \ddots & \vdots \\ \bar{n} & \cdots & 0 \end{pmatrix}\begin{pmatrix} b \\ \vdots \\ -\lambda \end{pmatrix} = \begin{pmatrix} d \\ \vdots \\ 0 \end{pmatrix} \quad (47)$$

Where $\bar{n}$ is the vector of the normalization integrals of fitting functions:

$$\bar{n} = \int f_\mu d\bar{r} \quad (48)$$

In practice, the vector of expansion coefficients b of $\rho^{(1)}$ is calculated in this way:

$$\bar{b} = \bar{t} - \frac{\langle\bar{n}|\bar{t}\rangle}{\langle\bar{n}|\bar{q}\rangle}\bar{q} \quad (49)$$

Where $\bar{t}$ is the solution of the linear Eq. (9) without any constrain, instead $\bar{q}$ is defined:

$$\bar{q} = (S-M)^{-1}\bar{n} \quad (50)$$

While ADF employs the full symmetry in both SCF and TDDFT parts, in the present method the symmetry is only partially exploited: the density fitting basis functions are not symmetrized; however, only the pairs of occupied (φ_i) and virtual (φ_a) orbitals involved in allowed dipole selection rules are actually considered.

We have implemented in the present method also the plasmon analysis according to Jacob et al.[30]: they suggested to study the evolution of the TDDFT photoabsorption spectra by changing a scaling factor $0 \leq \lambda \leq 1$ used to "turn on" the coupling matrix *K*. In present implementation this can be easily done multiplying the matrix *L* [Eq. (34)] by the scaling factor λ.

Computational Details

The LB94[31] or the Perdew Burke Ernzerhof (PBE)[32] exchange-correlation xc-functionals were employed to obtain the KS orbitals and eigenvalues from the KS equations, while the exchange-correlation kernel is approximated by ALDA[25] in the TDDFT part taking the derivative of the VWN[33] LDA xc-potential. The basis sets as well as the auxiliary density fitting functions employed consist of slater-type orbitals included in the ADF database. The new program allows a simple choice of a subset of the ADF fitting functions, to save computer time when some fitting functions are not necessary for an accurate description of the photoabsorption spectrum. Such choice was made with preliminary test calculations on the simple diatomic molecules Au_2, CS, and H_2 for Au, S, and H, respectively. The calculations have been performed at scalar relativistic level with Zero-Order Regular Approximation (ZORA).[34]

The structure employed in the present work is reported in Figure 2. It has been derived from that proposed in Ref. 35 by replacing the methyl groups with H atoms, symmetrising the obtained configuration in the D_5 point group symmetry and performing a DFT geometry optimization of the resulting configuration employing the LDA Vxc potential, except for the Au atoms whose coordinates were constructed to reproduce the experimental structure factor.[36]

To give a quantitative idea about the computational efforts and the efficiency of the spectrum calculation from the complex polarizability, for the $Au_{144}(SH)_{60}$ cluster the SCF

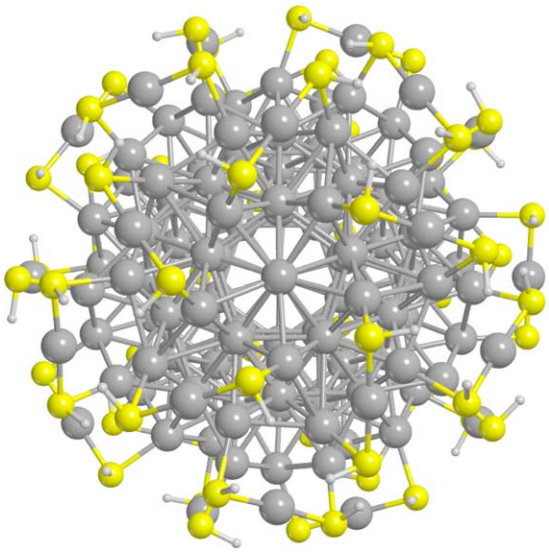

Figure 2. Structure of the $Au_{144}(SH)_{60}$ cluster in D_5 symmertry.

procedure employed 13 h using 16 cores on a Linux Infiniband Cluster with 8-cores Intel Haswell 2.40 GHz processors, while the resolution of the TDDFT inhomogeneous linear system (dim = 11628) employed only 172 seconds using 16 cores for each energy point. Since about one hundred of energy points are enough for a complete description of the spectrum, the TDDFT linear system resolution is one half of the SCF effort. In addition also matrix elements calculation time should be considered, so in general a TDDFT calculation will be comparable to a gradient calculation in terms of computational cost. One possible avenue for perspective development is to implement more efficient integration algorithms in the frequency space.

Application: The $Au_{144}(SH)_{60}$ Cluster

Monolayer-protected clusters with formula $Au_{144}(SR)_{60}$ have attracted a considerable interest in the literature, since the discovery of the stable and robust $Au_{144}(SCH_2CH_2Ph)_{60}$ species.[35] Such systems are in general quite appealing, since they can be produced in purely monodispersed form, thus allowing to combine the unique (e.g., plasmonic) response of metal clusters with a precise chemical composition. The $Au_{144}(SCH_2CH_2Ph)_{60}$ species in particular has been characterized by electrospray mass spectrometry, Scanning Tunnel Electron Microscopy,[37] and UV-vis absorption, albeit unfortunately it has not yet been characterized by X-ray diffraction, so its structure is not yet definitive although there are important indications which allow to build reasonable models. The first calculation of the optical spectrum of this cluster is reported in Ref. [19], in which the atomistic structure was taken from a previous work which assessed a widely used atomistic model.[38] In Ref. [19] the calculated photoabsorption was discussed in terms of TCM, such analysis pointed out a plasmonic behavior at 540 nm (2.3 eV) which was confined inside the cluster, while going to larger size the plasmon localizes on the surface. Another study[39] pointed out the richness of spectral features of the experimental absorption of $Au_{144}(SC_6H_{13})_{60}$, modelled by the simpler $Au_{144}(SCH_3)_{60}$ compound: a fair qualitative agreement was obtained between theory and experiment. A further systematic computational study[40] addressed the effect of structure, symmetry, anisotropy, exchange-correlation functional, R group, and charge state on the optical spectrum of $Au_{144}(SR)_{60}$ species. Very recently new low temperature (25 K) absorption experiments have been published as well.[41]

In the calculations here reported we use a $Au_{144}(SH)_{60}$ model structure which we derived in previous work.[36] We start the present analysis on $Au_{144}(SH)_{60}$ with a comparison between the spectra calculated at the TDDFT level with ADF code and the complex polarizability algorithm (Fig. 3): a good agreement is found between the two methods in the low energy interval of the spectrum, despite the limitation of the Davidson diagonalization of the Casida matrix employed by ADF which prevents to predict the spectrum at higher energy. In fact, the ADF spectrum reported in Figure 3 was obtained by extracting the 600 lowest eigenvalues of the Casida matrix, and it was not possible to go beyond this number without introducing numerical instabilities. The absorption intensity in the ADF spectrum is underestimated with respect to the complex polarizability prediction: this effect has been observed also in other systems and we attribute it to the missing background in the ADF results. In fact these systems are characterized by a strong absorption at higher energy (above 3 eV, see Fig. 4), which is completely absent in ADF since the extracted eigenvalues do not go beyond about 3 eV. On the contrary all the contributions are considered in the complex polarizability algorithm including the tails of the Lorentzian shape functions connected with the strong absorption above 3 eV which can influence and increase the background at small energy as well.

In Figure 4, we report the spectrum of $Au_{144}(SH)_{60}$ calculated at the TDDFT level with two different functionals (PBE and LB94) and basis sets (DZ and TZP). Since the cluster belongs to D_5 point group symmetry, there are only two non-equivalent electric dipole contributions: along Z (A_2) and along X or Y (E_1), which have been separately reported in the figure. The total absorption is obtained by summing the partial contributions weighted according to their degeneracy, and this

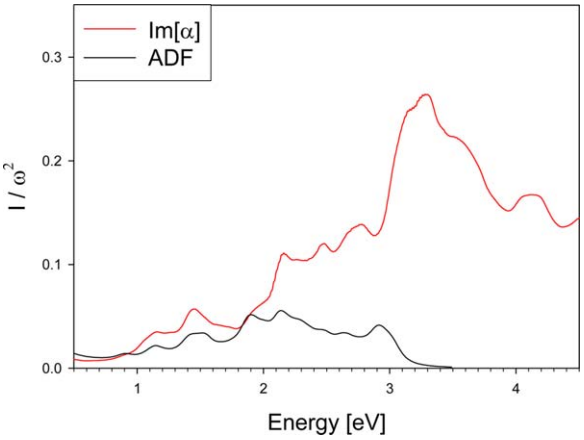

Figure 3. Calculated TDDFT photoabsorption spectra of $Au_{144}(SH)_{60}$. ADF (Davidson diagonalization) results compared with present complex polarizability algorithm.

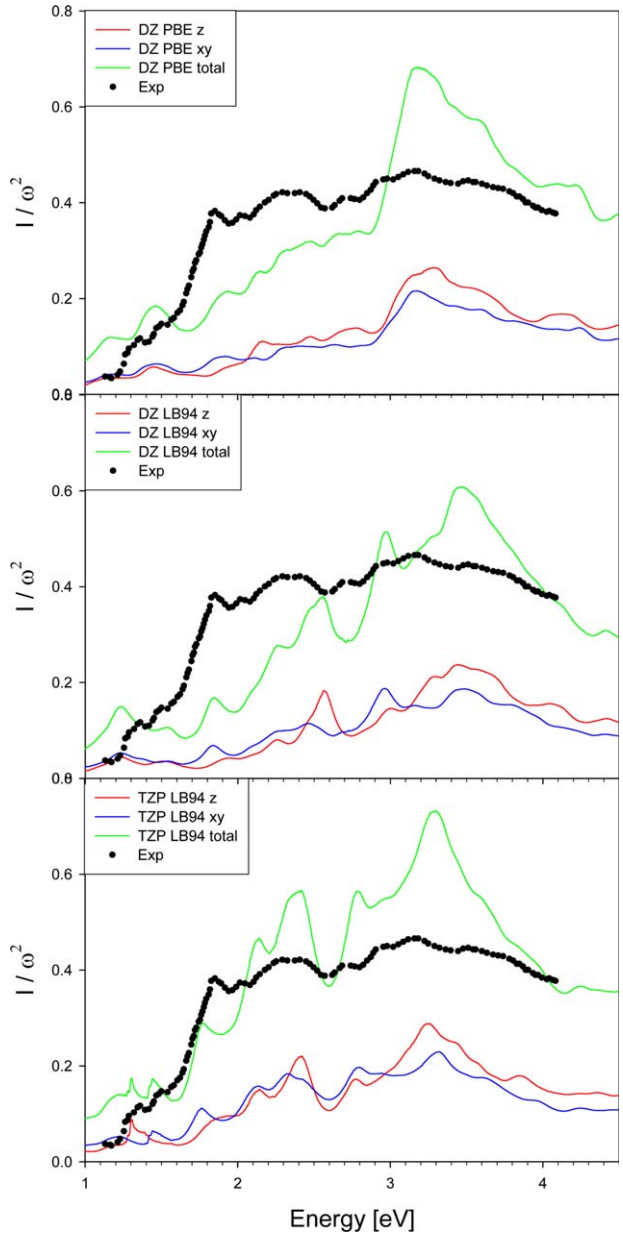

Figure 4. TDDFT photoabsorption spectra of $Au_{144}(SH)_{60}$ calculated by the complex polarizability algorithm. PBE-DZ, LB94-DZ, and LB94-TZP results are reported in the upper, central, and lower panel, respectively. Partial dipole components (*z* and *xy*) are given separately. Experimental data $Au_{144}(SC_6H_{13})_{60}$ at 77 K are reported.[39]

quantity is compared with the experimental data for $Au_{144}(SC_6H_{13})_{60}$ taken at 77 K.[39]

From Figure 4, it is apparent that the symmetry-equivalent *x* and *y* components of the absorption spectrum closely resemble the *z*-dipole component. This happens despite the fact that the ligands affect the geometry of the cluster, lowering the symmetry group from I_h to D_5. The difference between the components, also called anisotropy, is more pronounced at higher energy, where ligands play a more important role, while at low energy the spectrum is governed by the absorption of the gold core, which retains largely its icosahedral symmetry. In the low-energy region, the anisotropy is therefore less pronounced but still plays an important role, confirming that even these transitions are appreciably affected by the environment of the metal cluster.

Both xc-functionals with DZ basis set (upper and central panels of Fig. 4) give only a qualitative agreement with the experiment. In particular PBE displays a large upward jump around 3eV which is not supported by the experimental data. At lower energies both functionals display weak features which seem to reproduce correctly the experiment. However, the latter is characterized by a steep increase around 1.7 eV which is much more broadened in the calculated spectra. The oversimplification of the SC_6H_{13} into the SH ligands and the uncertainty in the cluster geometry prevent for a more detailed analysis and comparison between theory and experiment. However, it should be observed that the optical spectrum calculated using a TZP basis set and the LB94 Vxc potential (lower panel of Fig. 4) is in much better agreement with the experimental profile. Starting from the low-energy region, the predicted spectrum shows two weak signals at 1.3 and 1.5 eV in very good agreement with the experiment (1.36 and 1.50 eV). It is worth noting that these features are the result of the cluster anisotropy: in fact while the first peak at 1.3 eV is originated from the A_2 dipole component (along *Z*) the second one at 1.5 eV comes from the E_1 component (along *X* and *Y*). Interestingly such anisotropy effect is not present for the calculations with DZ basis set, showing that anisotropy is very sensitive to small details of the electronic structure and polarizability, whose accurate reproduction requires a larger basis set like TZP for a proper description. Going to higher energy, the theoretical data display a jump around 1.8 eV contributed mainly by the E_1 component, which corresponds to the above mentioned jump in experimental data at 1.86 eV. In this case the LB94 calculation with DZ basis gave the same assignment, albeit quantitatively less accurate. At higher energies the calculated spectrum is in worse quantitative agreement with the experiment, but the positions and the shape of the experimental profile are well reproduced by the theory, although the experiment is in general much smoother than the calculation. Namely there is a nice correspondence of maxima at 2.4, 2.7, and 3.2 eV, and also the dip at 2.6 eV is also very nicely reproduced. It is not easy to attribute the observed worsening of the theory as the energy increases: current effects might play a role due to the large size of the system but also basis set deficiencies may become more important as the energy increases.

Since we do not have absolute values for the experimental absorption intensities, our comparison is of course based on a rescaling and we cannot exclude an overall remodulation of the spectral weights.

Conclusions

We have described the implementation of a recently developed TDDFT algorithm based on the complex dynamical polarizability to calculate the photoabsorption spectrum of large metal clusters. Applications of the method are expected in the field of nanoplasmonics. The TDDFT equations are solved in

the space of the density fitting functions, so the problem is recast as a nonhomogeneous system of linear equations whose resolution need a numerical effort comparable to that of the SCF procedure. The construction of the matrix representation of the dielectric susceptibility is very efficient and is based on a discretization of the excitation energy, so such matrix is easily obtained at each photon energy value as a linear combination of constant matrix and energy-dependent coefficients.

The potentiality of the method is demonstrated by predicting the photoabsorption spectrum of the $Au_{144}(SH)_{60}$ monolayer-protected model cluster: when the LB94 Vxc potential and TZP basis are chosen, the agreement between theory and experiment is found to be quite nice.

The method is very promising, and several directions of development are envisaged. First, we expect to be able to deal with large metal clusters up to one thousand atoms and with low symmetry. Another promising avenue for algorithmic development lies in the inclusion of Hartree–Fock exchange in hybrid Vxc potentials, which could further improve the accuracy of TDDFT predictions. Another possibility is to implement more efficient integration algorithms in the frequency space. Further extension of the theory will be toward the implementation of the rotation strength to study dichroism of chiral clusters.

Acknowledgments

Computational support from CINECA supercomputing centre within the ISCRA programme is gratefully acknowledged. Computational research by A.F. was performed using PNNL Institutional Computing at Pacific Northwest National Laboratory.

Keywords: plasmonics · algorithm · metal clusters · time-dependent density-functional theory

[1] M. E. Casida, In *Recent Advances in Density-Functional Methods*; D. P. Chong, Ed.; World Scientific: Singapore, **1995**; p. 155.
[2] E. J. Baerends, D. E. Ellis, P. Ros, *Chem. Phys.* **1973**, *2*, 41.
[3] C. Fonseca Guerra, J. G. Snijders, G. te Velde, E. J. Baerends, *Theor. Chem. Acc.* **1998**, *99*, 391.
[4] S. J. A. van Gisbergen, J. G. Snijders, E. J. Baerends, *Comput. Phys. Commun.* **1999**, *118*, 119.
[5] O. Baseggio, G. Fronzoni, M. Stener, *J. Chem. Phys.* **2015**, *143*, 024106.
[6] K. Yabana, G. F. Bertsch, *Phys. Rev. B* **1996**, *54*, 4484.
[7] M. A. L. Marques, A. Castro, G. F. Bertsch, A. Rubio, *Comput. Phys. Commun.* **2003**, *151*, 60.
[8] A. Castro, M. A. L. Marques, D. Varsano, F. Sottile, A. Rubio, Comptes Rendus, *Physique* **2009**, *10*, 469.
[9] H.-Ch. Weissker, C. Mottet, *Phys. Rev. B* **2011**, *84*, 165443.
[10] X. López-Lozano, H. Barron, C. Mottet, Hans-Christian Weissker, *Phys. Chem. Chem. Phys.* **2014**, *16*, 1820.
[11] M. R. Provorse, C. M. Isborn, *Int. J. Quantum Chem.* **2016**, *116*, 739.
[12] B. Walker, A. M. Saitta, R. Gebauer, S. Baroni, *Phys. Rev. Lett.* **2006**, *96*, 113001.
[13] B. Walker, R. Gebauer, *J. Chem. Phys.* **2007**, *127*, 164106.
[14] D. Rocca, R. Gebauer, Y. Saad, S. Baroni, *J. Chem. Phys.* **2008**, *128*, 154105.
[15] P. Ghosh, R. Gebauer, *J. Chem. Phys.* **2010**, *132*, 104102.
[16] S. Grimme, *J. Chem. Phys.* **2013**, *138*, 244104.
[17] C. Bannwarth, S. Grimme, *Comput. Theoret. Chem.* **2014**, *1040*, 45.
[18] T. J. Zuehlsdorff, N. D. M. Hine, J. S. Spencer, N. M. Harrison, D. J. Riley, P. D. Haynes, *J. Chem. Phys.* **2013**, *139*, 064104.
[19] S. Malola, L. Lehtovaara, J. Enkovaara, H. Häkkinen, *ACS Nano* **2013**, *7*, 10263.
[20] M. Noda, K. Ishimura, K. Nobusada, K. Yabana, T. Boku, *J. Comput. Phys.* **2014**, *265*, 145.
[21] K. Iida, M. Noda, K. Ishimura, K. Nobusada, *J. Phys. Chem. A* **2014**, *118*, 11317.
[22] J. Neugebauer, *J. Chem. Phys.* **2007**, *126*, 134116.
[23] M. Pavanello, *J. Chem. Phys.* **2013**, *138*, 204118.
[24] M. Valiev, E. J. Bylaska, N. Govind, K. Kowalski, T. P. Straatsma, H. J. J. van Dam, D. Wang, J. Nieplocha, E. Aprà, T. L. Windus, W. A. de Jong, *Comput. Phys. Commun.* **2010**, *181*, 1477.,
[25] E. K. U. Gross, W. Kohn, *Adv. Quantum. Chem.* **1990**, *21*, 255.
[26] G. D. Mahan, K. R. Subbaswamy, *Local Density Theory of Polarizability*; Plenum Press: New York, **1990**
[27] M. Stener, P. Decleva, A. Lisini, *J. Phys. B At. Mol. Opt. Phys.* **1995**, *28*, 4973.
[28] M. Stener, P. Decleva, *J. Chem. Phys.* **2000**, *112*, 10871.
[29] R. Podeszwa, W. Cencek, K. Szalewicz, *J. Chem. Theory Comput.* **2012**, *8*, 1963.
[30] S. Bernadotte, F. Evers, C. R. Jacob, *J. Phys. Chem. C* **2013**, *117*, 1863.
[31] R. Van Leeuwen, E. J. Baerends, *Phys. Rev. A* **1994**, *49*, 2421.
[32] J. P. Perdew, K. Burke, M. Ernzerhof, *Phys. Rev. Lett.* **1996**, *77*, 3865.
[33] S. H. Vosko, L. Wilk, M. Nusair, *Can. J. Phys.* **1980**, *58*, 1200.
[34] E. van Lenthe, E. J. Baerends, J. G. Snijders, *J. Chem. Phys.* **1993**, *99*, 4597.
[35] H. Quian, R. Jin, *Nano Lett.* **2009**, *9*, 4083.
[36] G. Barcaro, L. Sementa, A. Fortunelli, M. Stener, *Nanoscale* **2015**, *7*, 8166.
[37] D. Bahena, N. Bhattarai, U. Santiago, A. Tlahuice, A. Ponce, S. A. Bach, B. Yoon, R. L. Whetten, U. Landman, M. Jose-Yacaman, *J. Phys. Chem. Lett.* **2013**, *4*, 975.
[38] O. Lopez-Achevedo, J. Akola, R. L. Whetten, H. Grönbeck, H. Hakkinen, *J. Phys. Chem. C* **2009**, *113*, 5035.
[39] H.-Ch. Weissker, H. Barron Escobar, V. D. Thanthirige, K. Kwak, D. Lee, G. Ramakrishna, R. L. Whetten, X. Lopez-Lozano, *Nat. Commun.* **2014**, *5*, 3785.
[40] H.-Ch. Weissker, O. Lopez-Acevedo, R. L. Whetten, X. Lopez-Lozano, *J. Phys. Chem. C* **2015**, *119*, 11250.
[41] Y. Negishi, T. Nakazaki, S. Malola, S. Takano, Y. Niihori, W. Kurashige, S. Yamazoe, T. Tsukuda, H. Häkkinen, *J. Am. Chem. Soc.* **2015**, *137*, 1206.

Accepted: 18 May 2016